

EFFECT OF CONCRETE CRUSHING ON FLEXURAL STRENGTH OF STEEL-CONCRETE COMPOSITE GIRDERS

Vivek Kumar GUPTA¹, Yoshiaki OKUI², Naofumi INABA³ and Masatsugu NAGAI⁴

¹Member of JSCE, Lead Structural Engineer, Chiyoda Corporation
(12-1, Tsurumichuo 2-chome, Tsurumi-ku, Yokohama 230-8601, Japan)
E-mail: vkgupta@ykh.chiyoda.co.jp

²Member of JSCE, Assoc. Prof., Dept. of Civil and Environmental Eng., Saitama University
(255, Shimo-Okubo, Saitama, 338-8570, Japan)

³Member of JSCE, Nippon Expressway Research Institute Company Limited
(1-4-1 Tadao, Machida-shi, Tokyo, 194-8508, Japan)

⁴Member of JSCE, Prof., Dept. of Civil and Environmental Eng., Nagaoka University of Technology
(1603-1, Kami-Tomioka, Nagaoka, Niigata, 940-2188, Japan)

The ultimate flexural strength of composite steel girders with compact sections is examined through experimental investigation and elasto-plastic finite displacement analyses to develop a reduction factor of the ultimate flexural strength. A two-point loading test of a composite girder was carried out to verify the numerical modeling by comparing the experimental and numerical results. Then, a parametric study was performed using finite element analyses to investigate the effect of concrete crushing on the flexural strength of composite girders constructed using SM570 grade steel. Observations made by comparison of the ultimate flexural strength obtained from the experimental and numerical results with that according to the AASHTO and Eurocode show that the existing reduction factor equations are conservative and can be relaxed when the strength is controlled by crushing of concrete slab. A new reduction factor for the ultimate flexural strength for composite I-girders under positive bending is proposed.

Key Words : reduction factor, ultimate flexural strength, composite I-girder, concrete crushing

1. INTRODUCTION

According to the American Association of State Highway and Transportation Officials (AASHTO) specifications¹⁾, composite sections with steel I-girders can be classified into three classes—compact, noncompact and slender sections—depending upon behavior of web plates in compression. The compactness requirements of Article 6.10.6.2.2 in AASHTO, originated mainly from the analytical and experimental work of Lay and Galambos^{2),3)}. Although adjustments were made for Load and Resistance Factor Design (LRFD) from the original proposal in American Institute of Steel Construction (AISC) code⁴⁾ by Yura *et al.*⁵⁾, where a rotation capacity of at least three is required, the rotation capacity requirement is not explicitly given in AASHTO. Accordingly, in this paper, the AASHTO's definition of compact sections will be adopted, which reaches its plastic moment capacity M_p without any rotation capacity requirement.

As in reinforced concrete theory, the ultimate flexural failure in composite compact sections can occur

either due to the yielding of steel in tension or crushing of concrete in compression. For compact sections in which the ductile failure takes place, the ultimate flexural strength is given by its full plastic moment capacity. However, for compact sections with higher steel yield strength, crushing of the concrete slab may take place prior to reaching the full plastic moment capacity of sections. The use of high strength steel in composite girders causes a deep position of the plastic neutral axis, which causes excessive compressive strain in concrete slabs and insufficient tensile strain in steel lower flanges at the ultimate state. Accordingly, in AASHTO and Eurocode⁶⁾, the design moment capacities for compact sections and class 1, 2 sections are reduced to avoid the concrete crushing. Furthermore, the position of the plastic neutral axis D_p (see **Fig. 1**) is restricted from the view point of ductility requirement.

One of the pioneering works on ductility of composite girders was done by Rotter and Ansourian⁷⁾ and Ansourian⁸⁾. They proposed a criterion to ensure ductility as $D_l/D_p > 1.4$, where D_l is called the limiting

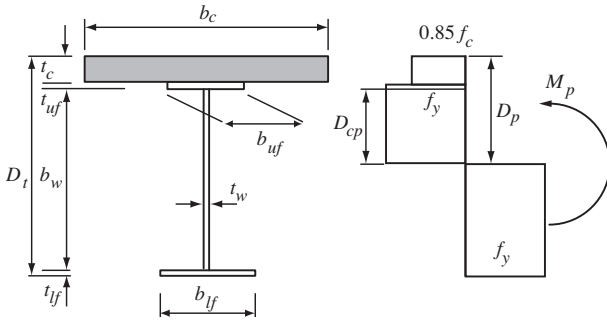


Fig.1 Stress distribution in compact section.

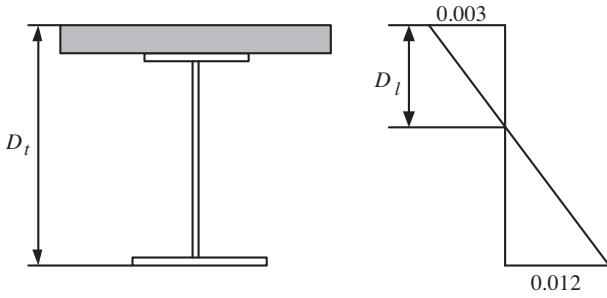


Fig.2 Assumed strain distribution in compact section⁸⁾.

neutral axis depth and defined from the strain distribution shown in Fig. 2 and D_p is the depth of the plastic neutral axis below the top of the concrete slab.

The 2001 AASHTO interim specifications⁹⁾ provided $D_p/D' \leq 5.0$ as a ductility requirement, where $D' = \beta D_t/1.5$ is defined as the depth of the plastic neutral axis when the maximum strain in concrete slab attains its crushing strain. The β factor was used to account for the effect of different steel grades on the ductility of composite sections and Ansourian's limiting value of 1.4 was rounded to 1.5 to ensure $D_p < D_t$.

In the 2005 interim revision of AASHTO specifications, a simple form of ductility ratio D_p/D_t is used, where D_t is the total depth of the composite girder. The previous ductility requirement $D_p/D' \leq 5.0$ corresponds to $D_p/D_t \leq 0.5$ where $D' = D_t/10$. The limiting D_p/D_t ratio is lowered to 0.42 in order to ensure ductile behavior. The value of $\beta=0.75$ was found to be good enough for all types of steel grades and hence adopted.

In view of the frequent modifications of the ductility requirement in AASHTO, the need for further investigation of ductility requirement becomes necessary. It is to be noted that the ductility requirement in Eurocode is given as $D_p/D_t \leq 0.40$.

Even though sections satisfy the ductility crite-

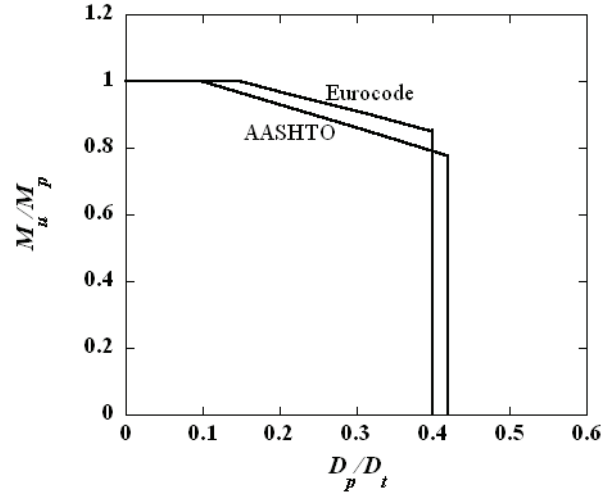


Fig.3 Strength prediction in AASHTO and Eurocode.

ria explained before, their ultimate flexural strengths have to be reduced from the full plastic moment capacity M_p due to concrete crushing. The design provisions in AASHTO for this strength reduction are based on the work of numerous investigators^{7),8),10),11)}. An analytical investigation was undertaken by Rotter and Ansourian⁷⁾ to check the experimental results of Chapman and Balakrishnan¹⁰⁾ for composite girders, which failed by crushing of concrete slabs. They presented a strength equation to determine M_u . However, the scope of their prediction equation is not clear. In the 2001 AASHTO interim specifications, the calculation of both plastic and yield moment capacities were required to evaluate M_u . Recently, Yakel and Azizinamini¹¹⁾ carried out experimental and analytical studies and developed an alternative strength equation, which requires less calculation for predicting M_u , because calculation of M_p was only needed. Their proposed method is reflected in the current AASHTO specifications, where a shorter and simpler form of strength equation has been used.

As shown in Fig. 3, the current AASHTO's equation for calculating M_u/M_p is given as:

$$\frac{M_u}{M_p} = 1.07 - 0.7 \frac{D_p}{D_t} \quad \left(0.1 < \frac{D_p}{D_t} \leq 0.42 \right) \quad (1)$$

Similarly, the Eurocode's equation for estimating M_u/M_p , less conservative than AASHTO's is given as:

$$\frac{M_u}{M_p} = 1.09 - 0.6 \frac{D_p}{D_t} \quad \left(0.15 < \frac{D_p}{D_t} \leq 0.4 \right) \quad (2)$$

It is to be noted that compact sections in AASHTO with $D_p/D_t \leq 0.1$ and class 1 and 2 sections with $D_p/D_t \leq 0.15$ in Eurocode can reach a minimum of M_p .

Table 1 Material test results for steel plates.

	yield strength [MPa]
Upper flange	313
Web	336
Lower flange	300

In this paper, the ultimate flexural strength of composite girders with compact sections was investigated by conducting a two-point loading test. The experiment results under positive flexure were used to verify the results of three-dimensional nonlinear FE analysis. An analytical parametric study, using FE models under positive bending is also presented. Details of the parametric study which aims to establish the design flexural strength equation are also reported. The ultimate flexural strengths obtained from experiment and numerical analyses were compared with the existing design equations. Finally, a new reduction factor for the ultimate flexural strength is developed and presented.

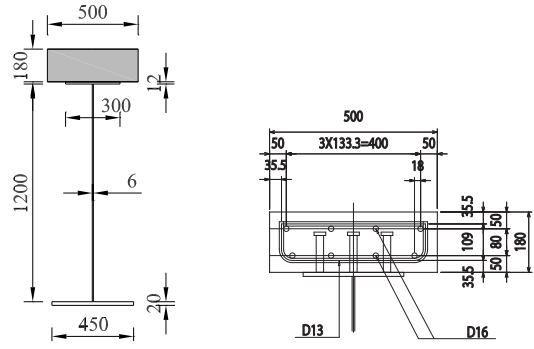
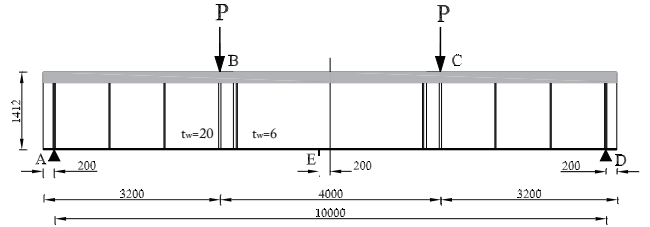
2. EXPERIMENTAL INVESTIGATION

The objective of the test is to determine the ultimate flexural strength of composite girder with a section qualified as compact sections. The experiment was performed in the structural testing laboratory of Komai Tekko Company.

(1) Test specimen and arrangement

A 10m long composite girder with a web depth-to-thickness ratio b_w/t_w of 200 was tested. The cross section dimensions are shown in **Fig. 4**. The composite girder has a 180mm thick RC slab. The test girder was designed so that it was classified as compact sections and that its plastic neutral axis lied in the web plate. The web slenderness $2D_{cp}/t_w$ based on material test results was 49.89, which satisfied the compact sections requirements of AASHTO and Eurocode; see **Fig. 1** for the definition of D_{cp} . The D_p/D_t ratio for the specimen was 0.242, which fell in the linear descending range of Eqs. (1) and (2). This value was selected to check the capability of AASHTO's and Eurocode's ultimate flexural strength equations to predict the strength governed by concrete crushing. The steel girder was made of steel grade SM400, whose material test results were shown in **Table 1** and the concrete used for the RC slab had a compressive strength of 44.3 MPa.

The test setup included two sets of a load cell over the hydraulic jack and displacement measurements at different locations. All measurements were taken using an electronic data acquisition system. The loading

**Fig.4** Cross-section dimensions of test girder, and details of re-bars [mm].**Fig.5** Composite girder under two-point loading [mm].

arrangement, which two symmetric point loads on the top of the concrete slab, produced a constant moment region between the loading points, as shown in **Fig. 5**. Since the experiment is primarily concerned with the flexural behavior of the girder, shear failure was prevented by installing vertical stiffeners on the web plate, and by increasing web thickness in the shear spans.

After the composite girder was ready to be tested, a two-point load device was attached on top of the girder. The behavior of composite girder in elastic, cracking, and inelastic ranges was carefully observed through a static test. The test girder was loaded in seven cycles with maximum loads of $P = 200, 400, 600, 800, 1100, 1600, 1800$ kN before ultimate load was reached. Both load and displacement control methods were applied for loading the girder. A photograph of the test setup is shown in **Fig. 6**.

(2) Test results

The load-displacement response of the tested composite girder is shown in **Fig. 7**. At the initial cycle of loading (i.e., within 11% of the ultimate load P_{ut}) the response is linear and no cracks were visible on the slab. As the load increased, the stiffness slightly decreased from the third cycle, but still no visible crack was observed on the surface of the concrete slab. During the seventh cycle, cracks begin to appear at the bottom of concrete slab. Finally, the failure took place



Fig.6 Test setup.

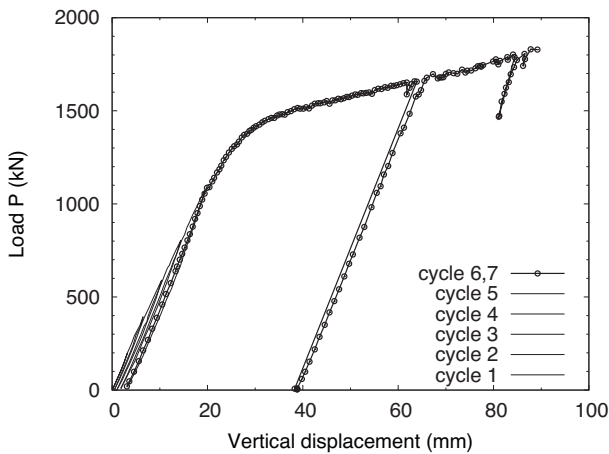


Fig.7 Load-displacement curve of test specimen; Vertical displacement is measured at point E in Fig.5.

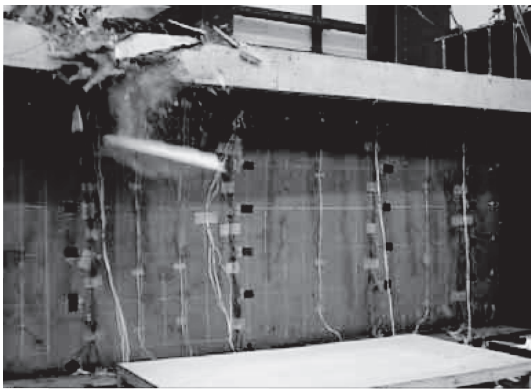


Fig.8 Typical crushing failure mode.

by crushing of concrete near one of the load points as shown in **Fig. 8**. The concrete crushing occurred within the constant moment region. No crushing was observed at the other locations.

Table 2 Results of experiment and its comparison with theoretical values.

Ultimate load P_u	1.81 MN
Ultimate moment M_u	5.42 MNm
Plastic moment M_p	5.03 MNm
D_p/D_t	0.242
M_u/M_p from exp.	1.08
M_u/M_p from Eq.(1)	0.902
M_u/M_p from Eq.(2)	0.916

Note: definition of M_p is shown in Fig.1.

Table 2 shows a summary of test results at failure condition, where the plastic moment M_p and the depth of plastic neutral axis D_p were calculated according to the rigid-plastic analysis theory. The concrete crushing occurred at a load of 1807kN, which represents the ultimate load of the specimen. Therefore, the ultimate moment M_{ut} is greater than M_p for girder with $D_p/D_t = 0.242$. This shows that sections with $D_p/D_t = 0.242$ can reach the plastic moment capacity M_p of the composite section without any ductility concerns. From the above results, it is interesting to note that the moment capacity of the test girder is much greater than those predicted by AASHTO and Eurocode ultimate flexural strength equations.

3. NUMERICAL SIMULATION OF EXPERIMENT

The FE analysis of the test girder under pure bending was carried out by using a nonlinear FE software¹²⁾. The primary aim of the numerical simulation was to validate the employed FE modeling by comparing with the experimental results.

(1) FE modeling

A three-dimensional FE model was developed to represent the tested specimen as shown in **Fig. 9** through the use of symmetry of the structural and loading conditions.

In the elasto-plastic finite displacement analysis, the brittle property of concrete is simulated with 8-noded solid elements that can change their stiffness depending on development of cracking and crushing of concrete and the steel girder is idealized by 4-noded isoparametric curved shell elements. The elements at the bottom of the concrete slab and mid-surface of the steel upper flange have common nodal points. Top and bottom longitudinal reinforcements have been modeled by the embedded element¹²⁾. The reinforcement consisted of two layers of D16 (15.9mm) reinforcing steel bars.

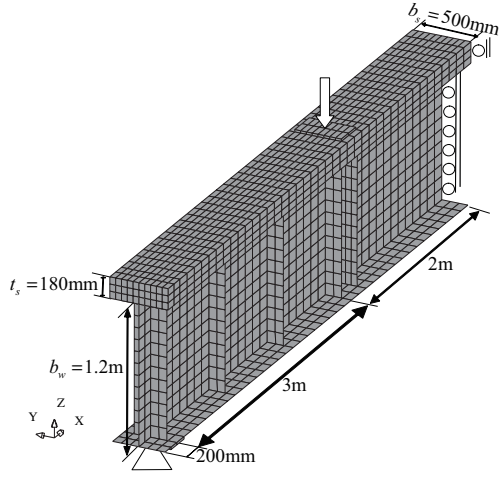


Fig.9 FE model of the composite girder.

(2) Material model

The FE analysis uses three sets of material properties for structural steel, reinforcement steel and concrete. These material models are described in the subsequent sections.

a) Structural steel

The uniaxial stress-strain relationships for steel shown in Fig. 10 were adopted. These stress-strain curves have three distinct regimes—elastic, distinct yield plateau and multi-linear strain hardening ranges, which are based on

$$\frac{\sigma_s}{f_y} = \frac{1}{\xi} \frac{E_{st}}{E_s} \left\{ 1 - \exp \left[-\xi \left(\frac{\varepsilon_{st}}{\varepsilon_y} - \frac{\varepsilon}{\varepsilon_y} \right) \right] \right\} + 1 \quad (3)$$

where σ_s and ε are the corresponding stress and strain of the steel respectively; f_y and ε_y are the yield strength and strain of steel respectively; E_{st} is the strain-hardening slope and $\xi = 0.02^{13}$. The von Mises yield criterion were employed. The associated flow rule and the isotropic strain hardening were used.

b) Reinforcement steel

The steel reinforcement was modeled as an elastic and ideally plastic material as shown in Fig. 10. The yield stress of the reinforcing steel was taken as 376MPa based on material tests.

c) Concrete

Concrete in compression is considered to be a linear-elastic, plastic and strain-softening material. The concrete material subjected to compressive stresses show pressure dependent behavior, i.e., the strength and ductility increase with increasing the hydrostatic pressure.

The Mohr-Coulomb failure criterion is employed as a yield criterion. The yield function for this failure criterion is expressed in terms of the principal stresses

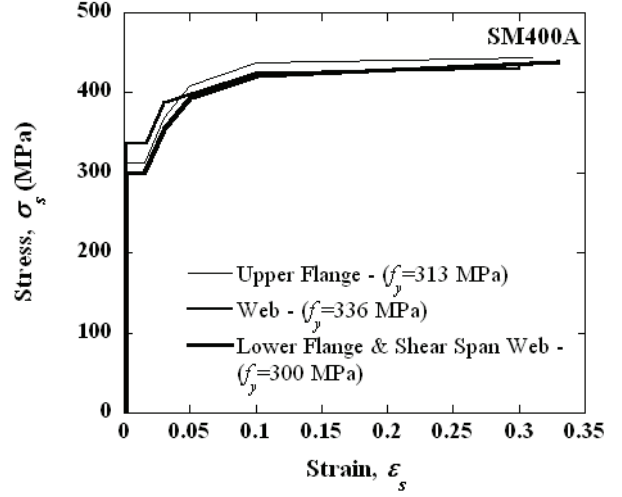


Fig.10 Stress-strain curve for structural steel.

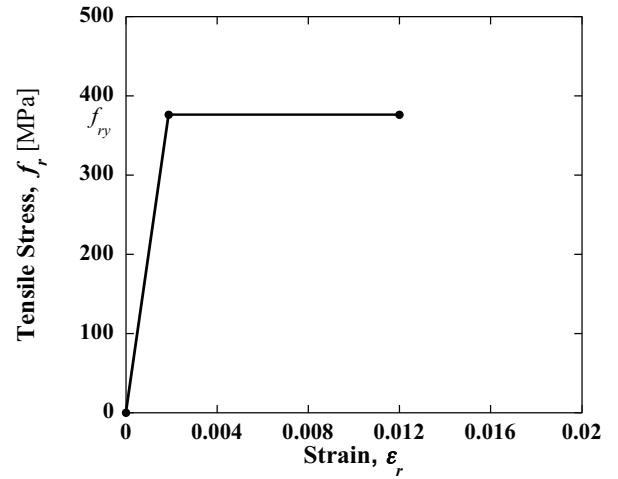


Fig.11 Stress-strain curve for reinforcement steel.

σ_i , ($i = 1, 2, 3$) as follows

$$F = \frac{1}{2}(\sigma_1 - \sigma_3) + \frac{1}{2}(\sigma_1 + \sigma_3) \sin \phi - c \cos \phi \quad (4)$$

where ϕ and c are the angle of internal friction and cohesion, respectively. The associated flow rule and the isotropic hardening are used in the analysis. The angle of internal friction is assumed to be constant $\phi = 20$ deg., while the cohesion is considered as a function of the equivalent plastic strain defined by

$$\bar{\varepsilon}_p = \int \sqrt{\frac{2}{3} d\varepsilon_{ij}^p d\varepsilon_{ij}^p} \quad (5)$$

where ε_{ij}^p stands for the plastic strain tensor, and the summation convention is used. The cohesion as a function of the plastic strain is obtained from a uni-

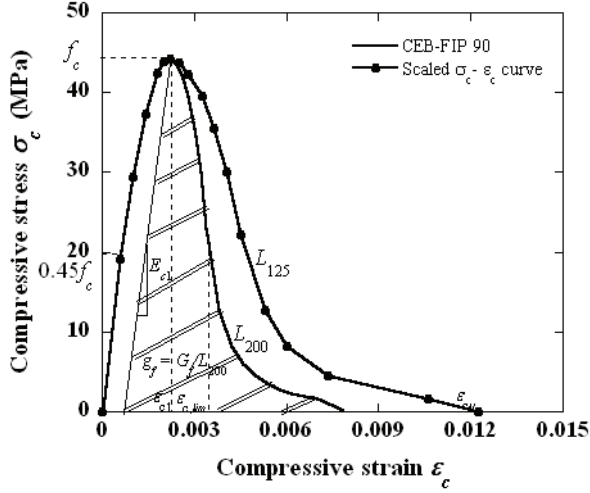


Fig.12 Size-consistent stress–strain curve for concrete.

axial stress-strain relationship and

$$c = \sigma_c \frac{1 - \sin \phi}{2 \cos \phi} \quad (6)$$

where σ_c is the compressive stress (positive in compression), which can be expressed as a function of the equivalent plastic strain.

The Comite Euro-International du Beton (CEB)¹⁴ has proposed the stress-strain model shown in **Fig. 12**, which includes the descending part of the stress-strain curve under uniaxial compression. This relation is composed of two parts: for $|\varepsilon_c| < |\varepsilon_{c,lim}|$

$$\sigma_c = \frac{\frac{E_{ci}}{E_{c1}} \frac{\varepsilon_c}{\varepsilon_{c1}} - \left(\frac{\varepsilon_c}{\varepsilon_{c1}}\right)^2}{1 + \left(\frac{E_{ci}}{E_{c1}} - 2\right) \frac{\varepsilon_c}{\varepsilon_{c1}}} f_c \quad (7)$$

and for $|\varepsilon_c| > |\varepsilon_{c,lim}|$

$$\sigma_c = \left[\left(\frac{\xi}{\frac{\varepsilon_{c,lim}}{\varepsilon_{c1}} - \frac{2}{\varepsilon_{c1}}} - \frac{2}{\varepsilon_{c1}} \right) \left(\frac{\varepsilon_c}{\varepsilon_{c1}} \right)^2 + \left(\frac{4}{\frac{\varepsilon_{c,lim}}{\varepsilon_{c1}} - \xi} \right) \frac{\varepsilon_c}{\varepsilon_{c1}} \right]^{-1} f_c \quad (8)$$

with

$$\xi = \frac{4 \left[\left(\frac{\varepsilon_{c,lim}}{\varepsilon_{c1}} \right)^2 \left(\frac{E_{ci}}{E_{c1}} - 2 \right) + 2 \frac{\varepsilon_{c,lim}}{\varepsilon_{c1}} - \frac{E_{ci}}{E_{c1}} \right]}{\left[\frac{\varepsilon_{c,lim}}{\varepsilon_{c1}} \left(\frac{E_{ci}}{E_{c1}} - 2 \right) + 1 \right]^2} \quad (9)$$

where ε_c is the compressive strain; $E_{ci} = 2.15 \times 10^4 (f_c/10)^{1/3}$ and $E_{c1} = f_c/\varepsilon_{c1}$ are the initial and secant moduli of elasticity respectively; $\varepsilon_{c1}=0.0022$ is the concrete strain at the peak compressive stress and f_c is the compressive strength of concrete and was taken as 44.3 MPa from material tests.

Since the post peak behavior is due to micro cracking in localized regions in an experimental specimen,

the descending portion of the stress-strain relation depends on the specimen length. Furthermore, it is well known that FE numerical results employing the strain softening plasticity present serious mesh dependency. A procedure known as fracture energy regularization was used to solve the mesh dependency or localization problem in FE analysis while modeling the strain-softening behavior of concrete in compression^{15),16)}.

The main idea of the regularization process is to modify the material softening behavior in such a way that the fracture energy integrated over the element is independent of the element length¹⁷⁾. The fracture energy in compression G_f is defined as

$$G_f = \int \sigma_c du_c^i \quad (10)$$

where u_c^i is the inelastic displacement. For general use of the fracture energy concept, it is better to rewrite Eq. (10) in terms of the specific fracture energy:

$$g_f = \frac{G_f}{L} = \int \sigma_c d\varepsilon_c^i \quad (11)$$

where L stands for the element length, ε_c^i is the inelastic compressive strain, and the integral represents the shaded area of the compressive stress-strain curve shown in **Fig. 11**.

Eqs. (7) to (9) represent the stress-strain relationship for an element length of 200 mm, while the concrete element length adopted in the FE analysis is 125mm.

Hence, for the FE model the descending part of the stress-strain curve was calibrated to maintain a constant fracture energy,

$$G_f = L_{200}g_f = L_{125}g'_f \quad (12)$$

in which $L_{200} = 200$ mm and $L_{125} = 125$ mm are the length of CEB-FIP 90 concrete element and the finite element length used in the analysis, respectively; and g_f and g'_f are the corresponding specific fracture energies.

From Eq. (12), we have

$$g'_f = 1.6g_f \quad (13)$$

and the scaled stress-strain curve used in the present analysis is shown in **Fig. 12**.

(3) Comparison of load vs. displacement plot

The load-displacement curve obtained from the numerical analysis is compared with the experimental one as shown in **Fig. 13**. Both numerical and experimental displacements are taken from the vertical deflection at the point E in **Fig. 5**, which is the bottom point and 200 mm left from the mid span. The loads corresponding to the yield and full plastic moments are plotted as the horizontal lines indicated by P_y and P_p , respectively. These yield and plastic loads

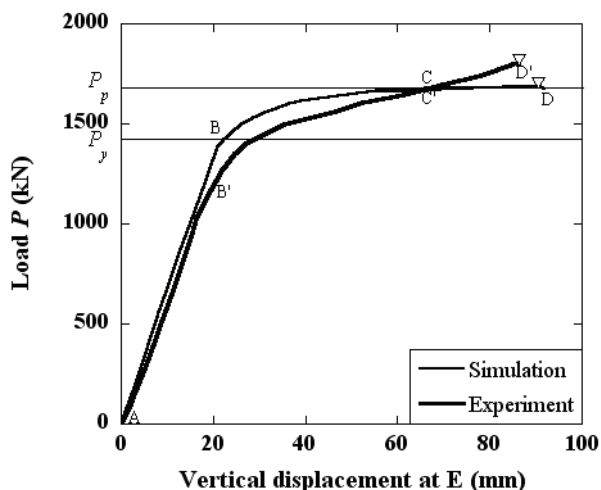


Fig.13 Comparison of load–displacement relationships at point E.

Table 3 Results of FE analysis.

Ultimate load P_u [MN]	Ultimate moment M_u [MN-m]	Yield load P_y [MN]	M_u/M_p
1.68	5.05	1.43	1.01

are calculated on the basis of the beam theory and the rigid-plastic assumption. The maximum loads in the load-displacement curves are defined as the ultimate loads P_u , which are indicated by the open triangles in **Fig. 13**.

It is found that, in the linear range, the load-displacement curve of the simulated FE model shows a trend almost similar to that of the experimental girder. However, in the nonlinear range, the response of FE model changes with increasing displacements compared to the experimental girder. It appears that the presence of residual stresses in the steel girder affects the behavior during the section B'C' of the experimental plot in **Fig. 13**. In general, the residual stresses cause initial yielding of the center portion of the bottom flange at a lower applied load. In this state, the stiffness of the experimental girder is less than that of the FE model, in which the residual stresses are not considered. At the points B and B', the lower portions of the steel girders start to yield, and at the points C and C', the loads attain the full plastic load of the composite section. At the point D' in the FE analysis, strain hardening was observed in the lower portion of the web plate but still 30% of the web plate behaved elastically. However, in the experimental specimen it appears that strain hardening

begins in the bottom flange at C' and may have spread through the steel girder until point D' is reached. At points D and D' the concrete can no longer sustain the any increase in applied loading and eventually fails by crushing; the applied loads attain their maximum values. These maximum bending moments are defined as the ultimate bending moments hereafter. The numerical results of the FE analysis are summarized in **Table 3**.

4. FINITE ELEMENT PARAMETRIC STUDY

With the aim presented in chapter 1, parametric studies have been carried out using FE method. A wide range of cross-section dimensions were examined and the numerical analyses were conducted on 35 composite girder models to investigate the effects of variations in geometry, such as the web depth-to-thickness ratio, on the flexural strength and ductility of composite girders. **Table 4**. summarizes the main section properties used in the parametric analyses.

The primary parameter varied in this study was D_p/D_t ratio and the sections were chosen to have D_p/D_t ratio in the range 0.15-0.4. In all of the chosen sections, the plastic neutral axes are located within the web of steel girders. Three b_w/t_w ratios 120, 150 and 200 were considered for nonlinear FE analyses. The sections with $b_w/t_w = 120, 150$ and 200 satisfied the compact section requirement proposed by Gupta *et al.*¹⁸⁾

$$\frac{2D_{cp}}{t_w} \leq 4.00 \sqrt{\frac{E_s}{f_y}} \quad (14)$$

where D_{cp} = depth of the web in compression at the plastic moment and t_w = thickness of the web, E_s = Young's modulus of steel and f_y = yield strength of steel.

The aspect ratio and depth of the web plates are assigned to 3 and 3m, respectively. Five concrete slab widths of 1.5m, 1.7m, 2m, 2.5m and 2.8m were chosen but its thickness was fixed to 300mm for all analyses. The upper flange width and thickness was varied between 300-700mm and 16-34mm, respectively whereas the lower flange width and thickness was varied between 650-850mm and 30-50mm, respectively. In the following sections, the analytical model and the results will be discussed.

(1) Analytical model

A 3D FE model simply supported at ends was selected for the parametric study. The symmetry of geometry and loading about the mid-span plane allows modeling of only half the length of the girder as

Table 4 Section properties.

Width-to-thickness ratio of web b_w/t_w	Girder	Upper flange [mm] $b_{uf} \times t_{uf}$	Lower flange [mm] $b_{lf} \times t_{lf}$	Slab [mm] $b_s \times t_s$	Ductility ratio D_p/D_t	Web slenderness $2D_{cp}/t_w$	M_u/M_p
200	1	450 × 20	700 × 30	2000 × 300	0.219	55.7	1.21
	2	400 × 19	750 × 35	2000 × 300	0.283	83.99	1.19
	3	400 × 20	750 × 45	2800 × 300	0.175	36.01	1.27
	4	350 × 18	700 × 45	2800 × 300	0.170	33.62	1.28
	5	300 × 16	650 × 50	2800 × 300	0.192	44.03	1.30
	6	700 × 32	700 × 32	1700 × 300	0.171	32.5	1.01
	7	600 × 33	700 × 32	1700 × 300	0.197	43.8	1.01
	8	700 × 32	700 × 32	1500 × 300	0.215	52.2	1.01
	9	650 × 33	700 × 32	1500 × 300	0.240	63.5	1.00
	10	500 × 34	700 × 32	1500 × 300	0.268	75.7	1.00
	11	550 × 33	750 × 34	1500 × 300	0.286	84.1	0.998
150	12	450 × 20	850 × 40	2500 × 300	0.306	70.83	1.01
	13	400 × 18	800 × 45	2500 × 300	0.333	80.33	1.01
	14	500 × 16	750 × 50	2500 × 300	0.336	81.64	1.01
	15	400 × 20	750 × 35	2500 × 300	0.256	53.96	1.02
	16	350 × 18	700 × 30	2500 × 300	0.230	45.82	1.02
	17	300 × 16	700 × 45	2000 × 300	0.317	74.82	1.01
	18	700 × 32	700 × 32	2000 × 300	0.208	36.7	1.01
	19	600 × 33	700 × 32	2000 × 300	0.227	43.2	1.01
	20	550 × 33	750 × 33	2000 × 300	0.257	53.2	1.00
	21	500 × 34	850 × 35	2000 × 300	0.303	68.5	0.998
	22	550 × 33	800 × 34	1700 × 300	0.325	76.3	0.994
	23	550 × 32	850 × 35	1700 × 300	0.348	84.0	0.993
120	24	500 × 16	750 × 50	2500 × 300	0.378	76.53	1.00
	25	450 × 20	700 × 40	2500 × 300	0.317	59.73	1.00
	26	400 × 20	750 × 45	2500 × 300	0.357	70.53	1.00
	27	500 × 20	700 × 45	2000 × 300	0.40	81.87	0.985
	28	450 × 20	700 × 40	2000 × 300	0.385	77.87	0.988
	29	400 × 22	750 × 38	2000 × 300	0.390	78.99	0.986
	30	700 × 32	700 × 32	2000 × 300	0.248	40.2	1.00
	31	550 × 32	750 × 33	2000 × 300	0.281	49.0	0.996
	32	700 × 32	700 × 32	2000 × 300	0.315	58.3	0.991
	33	600 × 33	750 × 32	2000 × 300	0.341	65.1	0.986
	34	550 × 34	800 × 35	2000 × 300	0.371	73.2	0.982
	35	500 × 32	850 × 36	2000 × 300	0.402	81.7	0.982

Note: Definitions of symbols are shown in Fig.1.

shown in **Fig. 14**. The bending moment loading was obtained by using forced rotation at the rigid end support about the major axis of the section. Constraints were applied at mid span to prevent the displacement in the girder axis direction. In the parametric study, the same elements as used for modeling the experimental girder are used.

For steel, the metal plasticity uses the von Mises yield criterion, the associated plastic flow, and the isotropic strain hardening. In this study, a multilinear stress-strain curve with and strain hardening was used (**Fig. 15**). The steel grade SM570 was employed. The residual stresses in steel girders have little effects on the ultimate bending moment^{19),20),21)} because of stress redistribution, so that they are not considered

in the analyses. However, the initial geometric imperfection of web plates may induce local buckling of the web plate, and thereby reducing the strength. Accordingly, the initial geometric imperfection was introduced into only the web plates in the nonlinear load-displacement analyses. The maximum initial displacement of $b_w/250$ that is the allowable maximum initial imperfection in the Japanese Specifications for Highway Bridges²³⁾ (JHBS) was introduced in the web plates.

The size consistent uniaxial stress-strain curve with compression softening behavior similar to one shown in **Fig. 12** is adopted. The curve also follows the CEB-FIP 90 stress-strain relationship and the concrete is assumed to have a compressive strength of

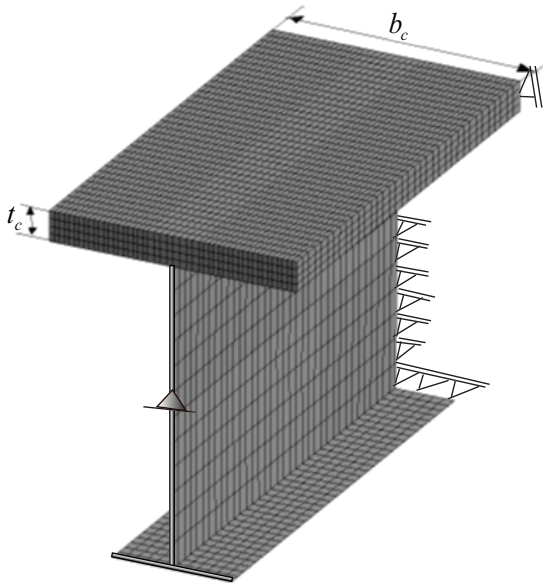


Fig.14 FE model of the composite girder for parametric study.

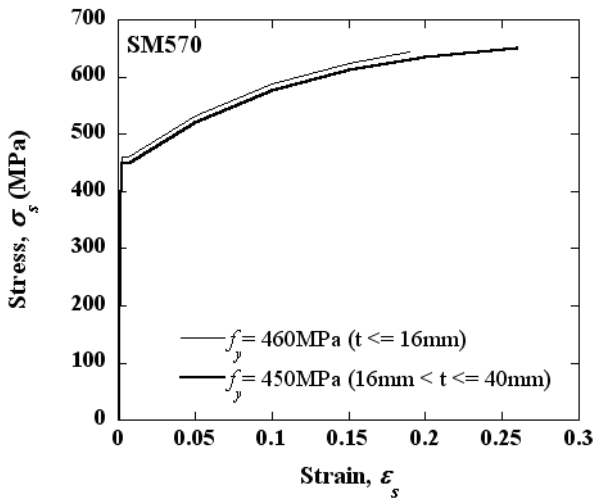


Fig.15 Stress–strain curve for steel grade SM570.

40MPa. The concrete material was modeled using Mohr-Coulomb model with the associated flow rule and the isotropic strain hardening.

(2) Parametric study results

The parametric study was conducted by changing D_p/D_t ratio, depth-to-thickness ratio of the web, width and thickness of the top and bottom flanges and width of concrete slab. **Table 4.** shows the results for selected composite girders, which failed by crushing of concrete. In parametric study, the ultimate flexural moment M_{up} is defined as the maximum value of bending moment obtained just before the bending moment tends to decrease with increasing curvature.

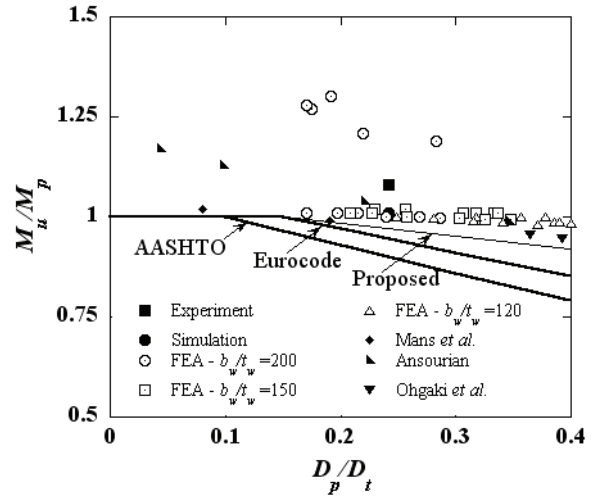


Fig.16 Relationship between M_u/M_p and D_p/D_t .

Nearly all of the girders except for a few girders either reached its plastic moment capacity or exceeded it. The girders with moderately high D_p/D_t ratios failed to reach their full plastic moment capacity. It is interesting to note that even for webs with $b_w/t_w = 200$, the full plastic moment capacity was obtained. It has also been found that, for girders having low web width-to-thickness ratios, the ultimate flexural strength reduces as the D_p/D_t ratio increases.

5. PROPOSED FLEXURAL STRENGTH EQUATION

Fig. 15 shows the plot between the non-dimensionalized ultimate flexural strength with respect to the full plastic moment capacity M_p and D_p/D_t ratio. The results of the present experiment, its simulation and the parametric analyses were compared with the existing experimental data reported by Ansourian⁸⁾, Ohgaki *et al.*²²⁾ and Mans *et al.*²⁴⁾. Ansourian employed European I beams called IPE 200 and 270 with total depths of 200 and 270 mm, respectively. Their depth-to-thickness ratios were 28 and 33. Hence, Ansourian’s specimens seem to be too small to represent composite girders used in recent composite girder bridges. The steel web depth of both Ohgaki’s specimens was 1420 mm, and the depth-to-thickness ratios of web plates were 118 and 157. Mans *et al.* used two specimens made of HPS-485W with yield strengths of 556-583 MPa; their web depth was around 760 mm, and depth-to-thickness ratios were 89 and 85. Details so these specimens, such as D_p/D_t ratio, are summarized in **Table 5.**

The current design equations (1) in AASHTO and (2) in Eurocode are plotted as the lines in **Fig. 16.**

Table 5 Summary of test results by other researchers.

Source	Specimen	D_p [mm]	D_p/D_t	M_p [kN-m]	M_u [kN-m]	M_u/M_p	Failure mode
Ansourian ⁸⁾	1	7.36	0.04	295	344	1.17	Slab crushing
	2	45.0	0.35	280	277	0.99	Slab crushing
	3	27.1	0.22	160	166	1.04	Slab crushing
	4	12.0	0.09	170	192	1.13	Slab crushing
Ohgaki <i>et al.</i> ²²⁾	MC1	586	0.36	7527	7178	0.97	Slab crushing
	MC2	630	0.39	7952	7522	0.95	Slab crushing
Mans <i>et al.</i> ²⁴⁾	POS1	189	0.19	5353	5304	0.99	Slab crushing
	POS2	80.5	0.08	4272	4369	1.02	Slab crushing

From the comparative plots shown in this figure, it can be seen that both AASHTO's and Eurocode's ultimate flexural strength equations are conservative, especially for D_p/D_t in the range 0.25-0.4. Although Eurocode's equation underestimates the flexural strength, it gives a fair estimation of the flexural strength for D_p/D_t between 0.15 and 0.20. Furthermore, the experimental result of POS1 specimen by Mans *et al.* closely agrees with Eurocode's strength equation. It is suggested, therefore, that the reduction factor for the ultimate flexural strength is predicted by the following equation:

$$\frac{M_u}{M_p} = \begin{cases} 1.00 & \left(\frac{D_p}{D_t} \leq 0.15 \right) \\ 1.05 - 0.33 \frac{D_p}{D_t} & \left(0.15 < \frac{D_p}{D_t} < 0.4 \right) \end{cases} \quad (15)$$

Eq. (15) gives a better estimate of the reduction factor for the flexural strength of composite girders with compact sections with D_p/D_t in the range 0.15-0.40.

6. CONCLUSIONS

In this study, all the girders were designed to verify the ability of the ultimate flexural strength equations provided by the current AASHTO and Eurocode specifications to predict the flexural strength of sections with D_p/D_t in the linear range. The selected girders have D_p/D_t in the range 0.15 to 0.4. Both experimental and analytical results show that the existing strength equations are conservative. Finally, an equation to estimate the reduction of ultimate flexural strength is developed and presented, which is found to be less conservative. The proposed equation is expressed as a function of D_p/D_t ratio. Moreover, the proposed equation gives a better estimate of the ultimate flexural strength of composite girders.

ACKNOWLEDGMENT: This investigation was carried out as a part of the activity of Technical Committee for enhancement of steel bridges performance in Japanese Society of Steel Construction. The Committee members valuable comments are gratefully ac-

knowledged. We would also like to thank Komai Tekko Inc. for offering their laboratory for conducting the reported experiment.

REFERENCES

- 1) American Association of State Highway and Transportation Officials (AASHTO), LRFD bridge design specifications - 2005 interim revisions, Washington, D.C. 2005.
- 2) Lay, M.G. and Galambos, T.V.: Inelastic steel beams under uniform moment, *Journal of Structural Division*, ASCE, Vol. 91, No. ST6, pp. 67-94, 1965.
- 3) Lay, M.G. and Galambos, T.V.: Inelastic beams under uniform moment gradient, *Journal of Structural Division*, ASCE, Vol. 93, No. ST1, pp. 381-399, 1967.
- 4) American Institute of Steel Construction (AISC), Specifications for structural steel buildings — load and resistance factor design (LRFD), Inc., Chicago, III, 1989.
- 5) Yura, J.A., Galambos, T.V. and Ravindra, M.K.: The bending resistance of steel beams, *Journal of Structural Engineering Division*, ASCE, Vol. 104, No. 9, pp. 1355-1370, 1978.
- 6) Eurocode 4: Design of Composite Steel and Concrete Structures, Part 2, Bridges 1, Draft, European Committee for Standardization (CEN), Brussels, Belgium, 1996.
- 7) Rotter, J.M. and Ansourian, P.: Cross-section behaviour and ductility in composite beams, *Proceedings of the Institution of Civil Engineers*, Part 2, Vol. 67, pp. 453-474, 1979.
- 8) Ansourian, P.: Plastic rotation of composite beams, *Journal of Structural Division*, ASCE, Vol. 108, No. 3, pp. 643-659, 1982.
- 9) American Association of State Highway and Transportation Officials (AASHTO), LRFD bridge design specifications - 2001 interim revisions, Washington, D.C. 1998.
- 10) Chapman, J.C. and Balakrishnan, S.: Experiments on composite beams, *The Structural Engineer*, Vol. 42, No. 11, pp. 363-383, 1964.
- 11) Yakel, A.J. and Azizinamini, A.: Improved moment strength prediction of composite steel plate girders in positive bending, *Journal of Bridge Engineering*, ASCE, Vol. 10, No. 1, pp. 28-38, 2005.
- 12) de Witte, F.C. and Kikstra, W.P.: DIANA Finite Element User's Manual: Analysis Procedures (release

- 8.1), TNO DIANA b.v., 2002.
- 13) Committee of new technology for steel structures: Guidelines and new technology for seismic design of steel structures, JSCE, 1996.
 - 14) Comité Euro-International du Béton: CEB-FIP Model Code 1990, Thomas Telford, 1993.
 - 15) Markeset, G. and Hillerborg, A.: Softening of concrete in compression – Localization and side effects, *Cement and Concrete Research*, Vol. 25, No. 4, pp. 702-708, 1995.
 - 16) Jansen, D. C. and Shah, S.P.: Effect of length of compressive strain softening of concrete, *Journal of Engineering Mechanics*, ASCE, Vol. 123, No. 1, pp. 25-35, 1997.
 - 17) Nakamura, H. and Higai, T.: Compressive fracture energy and fracture zone length of concrete, *Modeling of inelastic behavior of RC structures under seismic loads*, ASCE, pp. 471-487, 2000
 - 18) Gupta, V.K., Okui, Y. and Nagai, M.: Development of web slenderness limit for composite I-girders accounting for initial bending moment, *Doboku Gakkai Ronbunshuu A*, Vol. 62, No. 4, pp.854-864, 2006
 - 19) Ansourian, P., Roderick, J.W.: Analysis of composite beams, *J. of Struct. Dev., Proc. of ASCE*, Vol.104, No. ST10, pp.1631-1645, 1978.
 - 20) Egashira, K., Nakamura, S., Takahashi, K., Wu, Q.: Influence of steel properties on the positive flexural strength of steel-concrete composite sections, *J. of Struct. Eng.*, JSCE, Vol. 49A, pp. 791-798, 2003 (in Japanese).
 - 21) Ohgaki, K., Yasukawa, Y., Inaba, N. and Nagai, M.: Analytical study on elasto-plastic behavior of composite plate girder with large web aspect ratio and web depth-to-thickness ratio under sagging bending moment, *Proc. of The 5th Symp. on Research and Application of Composite Constructions*, Vol. 5, pp. 49-56, 2003 (in Japanese).
 - 22) Ohgaki, K., Kawaguchi, Y., Isoe, A., Takahashi, S., Kawashiri, K. and Nagai, M.: Experimental study on stiffening design method for main girder of composite plate-girder bridges, *Journal of Structural Engineering*, JSCE, Vol. 44A, pp. 1229-1239, 1998 (in Japanese).
 - 23) Japan Road Association: Specifications for Highway Bridges, Part II (Steel bridges), 2002.
 - 24) Mans, P., Yakel, A.J. and Azizinamini, A.: Full-scale testing of composite girders constructed using 485-MPa high-performance steel, *Journal of Bridge Engineering*, ASCE, Vol. 6, No. 6, pp. 598-604, 2001.

(Received July 13, 2006)